MSc in Photonics

PHOTONICS**BCN**

Universitat Politècnica de Catalunya (UPC)
Universitat Autònoma de Barcelona (UAB)
Universitat de Barcelona (UB)
Institut de Ciències Fotòniques (ICFO)

http://www.photonicsbcn.eu

Master in Photonics

MASTER THESIS WORK

CHARACTERIZATION OF A PARALLEL ALIGNED LIQUID CRYSTAL ON SILICON DISPLAY AND ITS APPLICATION ON A SHACK-HARTMANN SENSOR

Laura Lobato Bailón

Supervised by Dr. Juan Campos, (UAB)

Presented on date 15th July, 2010

Registered at

Escola Tècnica Superior d'Enginyeria de Telecomunicació de Barcelona

Characterization of a Parallel Aligned Liquid Crystal on Silicon display and its application on a Shack-Hartmann sensor

Laura Lobato Bailón
Laboratori de Tractament d'Imatges, Grup d'Òptica, Departament de Física, Universitat Autònoma de Barcelona, 08193 Bellaterra, Spain

E-mail: laura.lobato.87@gmail.com

Abstract. The characterization and the optimization of a parallel aligned liquid crystal on silicon display has been conducted with the aim to use it for the generation of a microlenses array in a Shack-Hartmann sensor. The entire sensor setup has been experimentally implemented from scratch. Measurements obtained for several wavefront aberrations prove the suitability of modulators in this particular application due to their dynamic properties, which easily allow for the proper choice of the sensor parameters.

Keywords: LCoS display, diffractive efficiency, Shack-Hartmann, Talbot effect.

1. Introduction

Liquid Crystal on Silicon (LCoS) displays are a subtype of Liquid Crystal Displays (LCDs) working by reflection. Some of the most noticeable features of these devices are their very high light efficiency and resolution, and also their great capability to spatially modulate light beams [1], this last being especially important in applications requiring phase-shift modulation of the incident wavefront. Consequently, they have attained widespread use in applications such as diffractive optics [2], adaptive optics [3], optical metrology [4], polarimetry [5] or medical physics [6].

In this framework, complete LCoS characterization and optimization becomes essential so as to achieve better performance of these devices and thus provide greater efficiencies in diffractive optics. In this article, the characterization of the LCoS display and its optimization comprises both the selection of the best electrical sequence providing the maximum efficiency in diffractive applications and also the determination of the aberrations of the silicon substrate of the device.

The main part of the work focuses on the experimental implementation of a Shack-Hartmann sensor in which the lens array has been generated by means of the LCoS display. Results obtained enjoy a remarkably importance because of the vast use of Shack-Hartmann sensors, currently used in fields so varied such as ophthalmology [7], astronomy, adaptive optics [8], optical alignment and commercial optical testing [8]. Furthermore, the dynamic generation of the lens array may present many advantages when compared to typical arrays of lenses as they could enhance lateral resolution without implying dynamic range losses.

The outline of the paper is as follows: In Section 2 we deal with the characterization of the modulator, where the best electrical sequence providing the maximum diffractive efficiency has been selected and aberrations of the silicon substrate have been determined. Section 3 is divided into two subsections. The first one corresponds to a Matlab simulation of the Shack-Hartmann

sensor while the second part presents the results experimentally obtained at the laboratory. Finally, the main ideas of the paper are summarized in Section 4.

2. Characterization of the PA LCoS

In this section, we present the results of the characterization of a PA LCoS, which has been conducted with the aim to achieve better efficiencies in diffractive applications. In particular, two phenomena are considered: the effect that electrical pulse schemes have on the diffractive efficiency and also the aberrations appearing on the LCoS reflected light as a consequence of the non-totally flatness of the silicon substrate. The substrate's irregular shape results in a systematic error addition to the reflected rays. In order to increase the diffractive efficiency, the optimum electrical sequence must be addressed to the modulator and aberrations must be counteracted by properly addressing a calibrated phase function.

2.1. Electrical pulse scheme

While most commercial LCDs do not offer the chance to access the parameters defining the electrooptic modulation properties of the LC device, the PA LCoS used in this study allows different electrical sequences formats to be addressed, which may also result in different responses and efficiencies [9]. Modern LCoS displays are digitally addressed, and the electrical sequences are based on pulse-width modulation scheme. The modulated pulses can lead to flicker in the optical beam because of the limited viscosity of the LC molecules, which restrict them to following one single pulse at a time. This may introduce undesirable temporal phase fluctuations [10] on the light beam reflected by the LCoS display. Because this phenomenon has a marked tendency to deteriorate the LCoS performance in diffractive optics, we endeavour to analyze the modulator performance as a function of four different electrical pulse schemes.

This study has been undertaken for a 633nm laser light source and for quasi-normal incidence. The light modulator used is a PA LCoS display distributed by HoloEye. The modulator works by reflection, therefore enabling a higher dynamic modulation range when compared to previous LCoS displays because of the double pass of the light through the device. It also presents a high resolution due to its 1920x1080 pixel screen; a high fill factor of 87% and a pixel size smaller than 8µm.

The electrical sequence providing the best efficiency corresponds to the one minimizing phase fluctuations and maximizing the available phase-shift. The following graph shows the retardance curves as a function of the gray level for each one of the four sequences. These have been obtained from the experimental Mueller matrices and by applying afterwards the polar decomposition in order to get the Jones matrices [11].

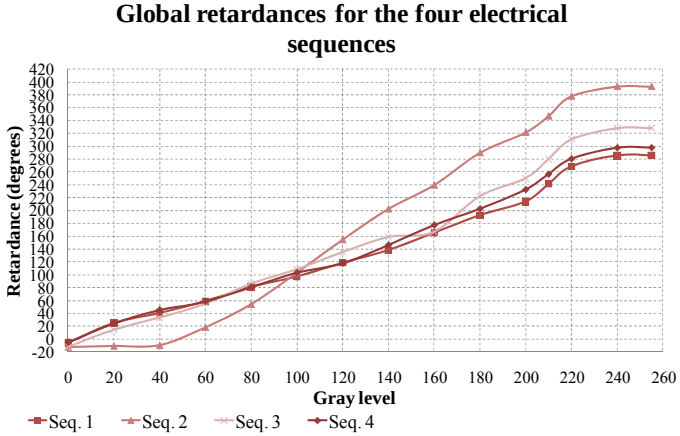

Figure 1. Phase-shift as a function of the gray level for the four electrical sequences considered.

From the graph above, sequences 1 and 4 can be already ruled out after showing too short retardances so as to be successfully used in diffractive applications. The efficiency of the other two sequences has been studied by generating diffractive optical elements (DOEs) into the LCoS display. As sketched in Fig. 2., the LCoS display is impinged with an unexpanded He-Ne

laser beam at quasi-normal incidence (2°). Light coming from the laser goes through a half wave-plate (HWP0) which enables to control the light intensity. A polarizer is set at the entrance of the incident beam in order to generate linearly polarized light being parallel to the LC director axis. In this way, the modulator is working with a phase-only regime and depolarization effects can be removed. Another polarizer set in the same position is placed at the exit of the beam. After the last polarizer, two photodetectors are placed in a far diffraction plane, gathering both the zero and the first diffraction order intensities in synchronization. DOEs generated correspond to both binary and Blazed gratings.

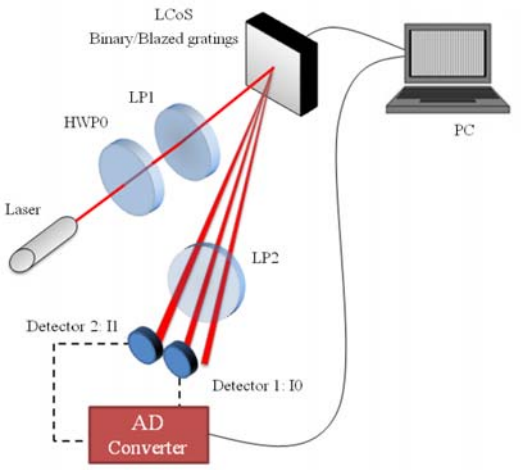

Figure 2. Optical setup to capture the zero and first order intensities when generating diffractive gratings.

It can be mathematically proved [10] that when working with a phase π for an ideal binary grating, provided that fluctuations in time are neglected, the zero diffraction order shows an intensity value equal to zero while the first two diffraction orders each register 40% of the total intensity. Furthermore, from the zero and first diffraction order intensities, the instantaneous phase can as well be obtained [10], providing information about time-fluctuations for the specific case of a π phase-shift. Fig. 3. shows the results obtained for the sequence 2 and 3.

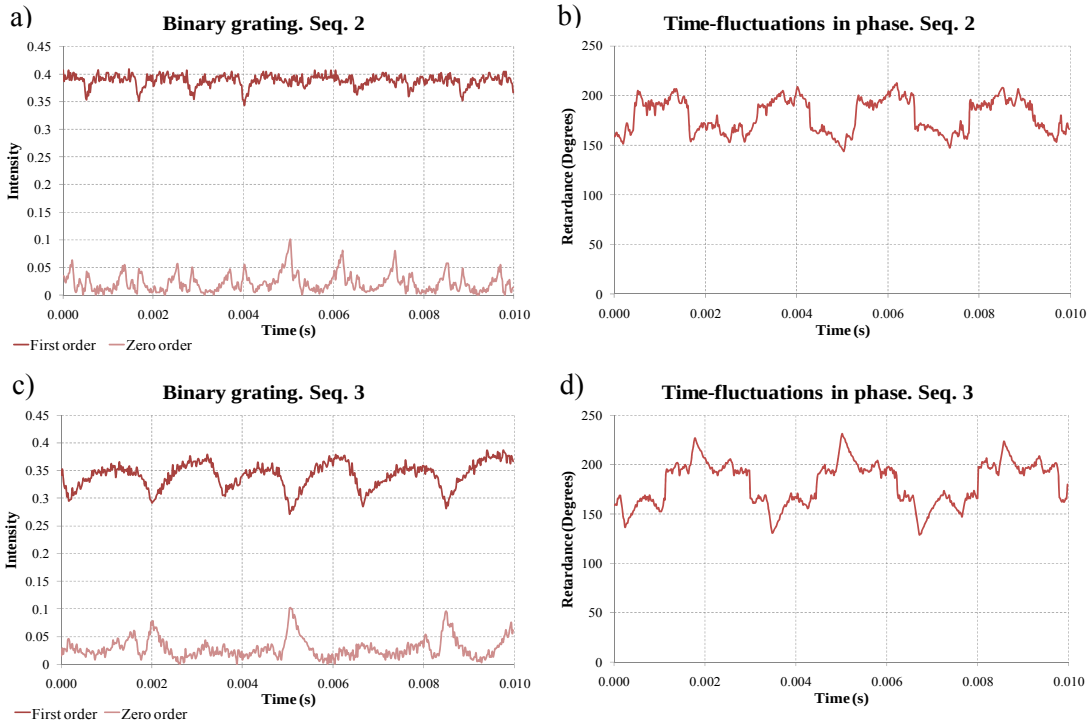

Figure 3. a) Binary grating for the sequences 2. b) Time-fluctuations of the sequence 2 for a phase-shift of π.
c) Binary grating for the sequence 3. d) Time-fluctuations of the sequence 3 for a phase-shift of π.

We can observe that for a binary grating providing a phase-shift of π, sequence 2 results in a better efficiency than sequence 3, with an intensity value almost reaching 40% of the total intensity for the first order diffraction. Time-fluctuations in phase also result being smaller for sequence 2 than for sequence 3, with a pick-to-valley value of approximately 50º in the former case while almost 70º are reached in the case of sequence 3.
On the other hand, when generating Blazed gratings, several gray levels are being addressed to the modulator, *i.e.* the element generated contains different phase-shifts. Therefore, from intensities gathered, the LCoS general behaviour can be observed. Intensities for the Blazed gratings are shown in Fig. 4:

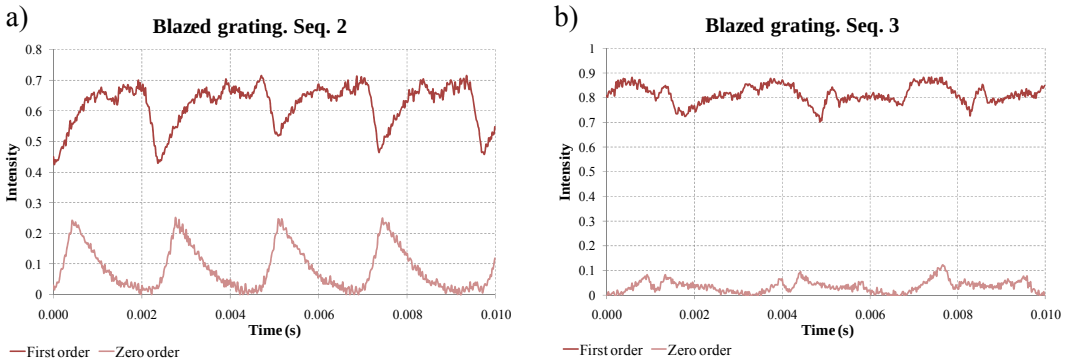

Figure 4. Zero and first order diffraction intensities for the Blazed gratings corresponding to: a) Sequence 2. b) Sequence 3.

In this case, we can observe that sequence 3 behaves better than sequence 2 since it shows an intensity value of 90% of the total intensity for the first order of diffraction while sequence 2 barely reaches 70% and presents much wider pick-to-valley values. This suggests that sequence 2 has been optimized to work with a phase-shift of π, while it does not succeed in working at other retardances. Since modulator applications often require from the generation of diffractive elements containing several gray levels, sequence 3 has been chosen as the electrical pulse scheme providing the best trade-off between global retardance (not reaching 2π but still high enough) and time-fluctuations in phase.

2.2. Modulator aberrations

Silicon substrate aberrations of the modulator have been determined by applying the phase-shifting interferometry. This method is a common optical technique for non-contact surface profilometry which requires the surface being quite smooth.
The experimental setup implemented is a Michelson interferometer, shown in Fig. 5. Light coming out from the laser crosses a half waveplate and a linear polarizer. With these two elements we attenuate the beam intensity and also generate the required state of polarization to enter the PA LCoS. After that, a spatial filter is placed in order to both remove the noise and also expand the laser beam. Light is collimated by a lens and divided into two beams by the beam splitter. One of them travels until the PA modulator under test and the other one is directed to the movable mirror. This device is a piezoelectric which can be moved forwards and backwards depending on the applied voltage. Light is then reflected by the modulator and the mirror and recombined again into the beam splitter. From here, light travels until the camera, where the interference pattern is gathered.
Different positions for the movable mirror also result in different optical paths being travelled by the light in this direction. Therefore, for each position of the mirror, the phase difference between the two recombined beams will be different and as a consequence, different interferograms will be obtained. Four interferograms have been experimentally taken, each one performed after displacing the mirror π/2 in terms of phase. With these four interferograms, the optical surface of the PA LCoS can be mapped by applying the following expression [12]:

$$\Phi = a\tan\left(\frac{I_{\pi/2} - I_{3\pi/2}}{I_0 - I_\pi}\right), \tag{1}$$

where Φ is the phase of the modulator silicon substrate and I_0, $I_{\pi/2}$, I_π and $I_{3\pi/2}$ refer to the four successive interferograms. The modulator aberrations are shown in Fig. 6.

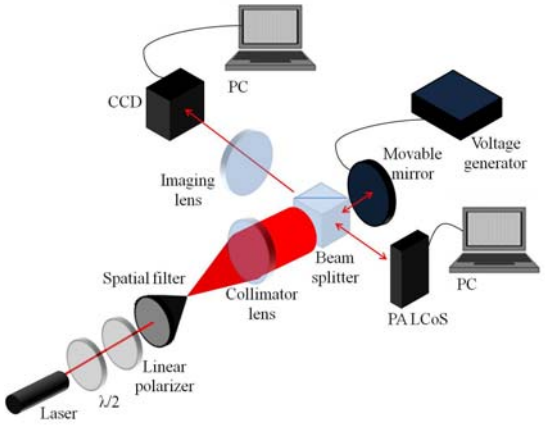

Figure 5. Michelson setup used to determine the aberrations of the silicon substrate of the PA LCoS.

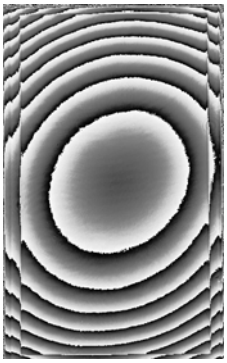

Figure 6. Aberrations from the silicon substrate of the PA LCoS, which have been found by making use of a Michelson interferometer and by applying afterwards the phase-shifting interferometry.

Once the topography of the silicon substrate has been obtained, the modulator efficiency can be increased by addressing to the modulator the exact inverse phase function so that a completely flat wavefront is obtained after light reflects onto the modulator.

3. Simulation and experimental implementation of a Shack-Hartmann sensor

The last part of this work relates to the experimental implementation of a Shack-Hartmann sensor. The novelty lies in the generation of the lens array by means of the LCoS device once it has been characterized as stated in the previous section. Modulators present many advantages with respect to conventional lenses when it comes to designing a lens array because they are dynamic. By successive displacements of the lens array, the dynamic range of the Shack-Hartmann sensor may be greatly enhanced without resulting in the lateral resolution losses already reported by some authors [8].

In the first subsection, we have computed a Shack-Hartmann sensor with the Matlab programming language because simulations usually allow an easy approximation to the kind of results we will afterwards obtain at the laboratory. In the second subsection, the experimental implementation of the Shack-Hartmann sensor is conducted and the results obtained are presented.

3.2. Theory and simulation development

The Shack-Hartmann sensor is made up of two main components: an array of microlenses set at the entrance pupil of the system and a light detector placed at the focal plane of the lens array. Considering an initial flat wavefront, it will form a reference image of dots in the microlenses focal plane, which will be perfectly squared if the lens array distribution is also squared. Aberrations of the incident wavefront result in local slopes which will displace the dots from the reference position, thus providing information about the real aberration of the initial wavefront. In Fig. 7. the Shack-Hartmann sensor is sketched.

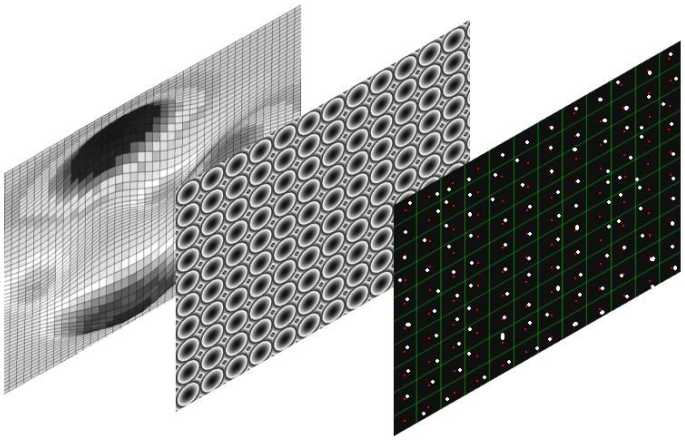

Figure 7. Shack-Hartmann sensor. For the aberrated incident wavefront, the obtained dots (white spots) are displaced from the reference dots (red spots).

The Matlab simulation considers the following parts:

3.2.1. Initial wavefront and microlenses array

Aberrated wavefronts can be created by selecting a term from Zernike polynomials. After that, each one of the microlenses of the array adds a quadratic phase to the initial wavefront. The total added phase can be expressed as follows:

$$\varphi = \sum_{n}^{N} \sum_{m}^{M} \exp\left(\frac{i\pi\left((x-na)^2 + (y-ma)^2\right)}{\lambda f} \right) \cdot rect\left(\frac{x-na}{a} \right) rect\left(\frac{y-ma}{a} \right), \tag{1}$$

where φ is the phase introduced, λ is the light wavelength, f is the focal length, x and y are the spatial coordinates, a is the microlens aperture and n and m refer to the particular microlens adding the phase. The user can set the suitable optical parameters of the SH sensor so that good results for the particular wavefront measurement can be obtained. These parameters include the illumination wavelength, the focal length of the microlenses and also their aperture.

The most important parameter is the focal length because it directly influences the dynamic range of the setup and its measurement accuracy. Longer focal lengths imply more sensibility to small aberrations of the incident wavefront but they also entail a smaller dynamic range because of the higher deviation rays undergo when compared to shorter focal lengths [13].

The microlenses aperture is another parameter to take into account when it comes to increasing the dynamic range. Bigger apertures increase the dynamic range because they allow larger beam deviations. However, it is not advisable either to work with too big apertures because in this case, the lateral resolution decreases due to the small wavefront sampling and therefore the wavefront curvature cannot be neglected inside one single aperture [13].

Regarding the light wavelength, shorter wavelengths reduce diffraction effects and also enhance the lateral resolution because they allow working with smaller apertures [13].

3.2.2. Free propagation and spots location

The wavefront propagation through the free space from the microlenses array until the CCD can be calculated by means of the Fresnel propagation. It makes use of the Transfer function of the free propagation, which is given by:

$$\varphi_{prop} = \exp(ikz)\exp\left(i\pi\lambda z\left(u^2+\upsilon^2\right)\right), \tag{2}$$

where z is the distance that light must travel and u and υ are the frequencies in the x and y directions respectively, since the propagation is calculated in the Fourier domain.
Once the wavefront has been propagated until the CCD, we need to average the spots intensity since the camera pixel is usually greater than the sampling size. Consequently, an energy average is required which will depend on the relationship between the sampling distance and the camera pixel size.
The spots location is often the weakest point of SH sensors and so, in order to reduce errors in the wavefront measurement, a good centroid estimation is required. The problem with centroid estimation lays in the fact that the irradiance pattern of the microlenses array usually consists of not only the main spots from each lens, but also of some secondary spots between main dots, which are caused by the diffraction of the small size of the lenses and by the interference from different microlenses. As a consequence, there is an additional error to the centroid estimation.
The $F^{\#}$ gives a relationship between the focal length and the lens aperture, and it can be written as:

$$F^{\#} = \frac{f}{a}. \tag{3}$$

This expression gives an idea of how big the additional error will be. For large $F^{\#}$ (small lenses with long focal lengths) the number of spots between two main spots, N, decreases [14]:

$$N = \frac{1}{F^{\#}}\frac{a}{\lambda} - 2. \tag{4}$$

In general, the additional error is larger for smaller N numbers since in these cases, each secondary spot receives a lot of energy, and thus the difference between main spots and secondary spots becomes less noticeable, making harder to locate the spot centroid. Therefore, a suitable choice for the focal length of the microlenses and their apertures becomes once again of high importance.

3.3. Experimental results

The setup used in this part basically consists of three main parts. As sketched in Fig. 8., the first part includes a LCoS display from Philips, model X97c3A0, sold as the kit LC-R2500 by HoloEye. It is a twisted nematic LCoS with a screen resolution of 1024x768 pixels, a pixel center to center separation of 19μm and a fill factor of 93%. A polarization state generator (PSG) is placed at the incident beam, composed by a linear polarizer and a quarter waveplate. A polarization state detector (PSD) made up of a quarter waveplate and an analyzer has as well been placed at the exit of the beam. The suitable configuration for the PSG and the PSD yields a phase-only modulation with maximum transmittance [10]. This modulator allows creating aberrated wavefronts by introducing coefficients from Zernike polynomials. Being able to create known aberrations becomes essential since it gives the capability to predict how much spots will displace from the reference spots and in which direction they will do it.
After exiting the PSD, light travels until the PA LCoS. As stated in Section *2.1.*, light must enter the modulator parallel to the LC director axis in order to remove depolarization effects. Therefore, a half waveplate conveniently arranged must be placed just at the entrance of the display. In the PA LCoS, the array of microlenses is created from a software. Light goes into the display and is reflected back to the camera thanks to a beam splitter.
The last part of the setup consists of a CCD placed on a rail so that it can be displaced forwards and backwards in such a way that the spots pattern can be properly focused.

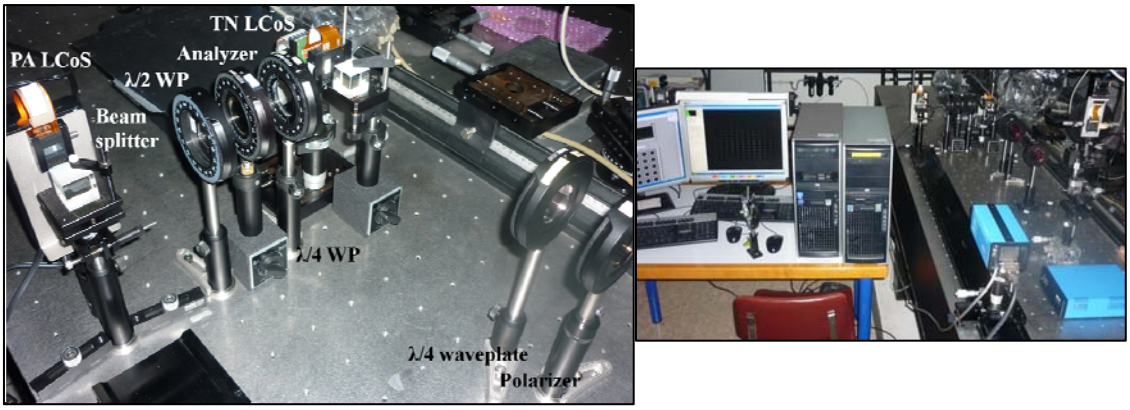

Figure 8. Set up of the Shack-Hartmann sensor used to measure the wavefront aberration created by the TN LCoS.

Experimental microlenses have been generated with an aperture of 100 pixels and a focal length of 100 mm. This microlenses configuration generates the best possible pattern of spots since smaller focal lengths are not sensible enough to slight wavefront aberrations and smaller apertures do not allow for the proper lens generation within the PA LCoS display (too few rings are generated therefore).

By making use of the Talbot effect, the dots pattern can be gathered at several distances from the PA LCoS. The Talbot distance, Z_T, at which the first self-image is obtained, can be written as [15]:

$$Z_T = \frac{2a^2}{\lambda}, \tag{5}$$

where a is the microlens aperture and λ is the illumination wavelength. In our case, the Talbot distance is 20.25 cm. At some fractions of the Talbot distance, we do not find exact copies of the initial image but images appear with some variations: there is a period shifting at half of the $\mathbf{Z_T}$ and frequency doubles at a $\mathbf{Z_T}/4$. In order to determine the best working distance at which wavefront measurements should be performed, we generate a vertical linear phase into the twisted nematic display and compare the displaced patterns obtained at three different distances corresponding respectively to the one where the self-image appears, the one showing a double spots frequency and also the distance where the spots frequency triplicates. Spots are assumed to move on the y axis because of the linear phase introduced. Fig. 9. shows the distances between reference spots and displaced spots for the self-image and for the triple frequency.

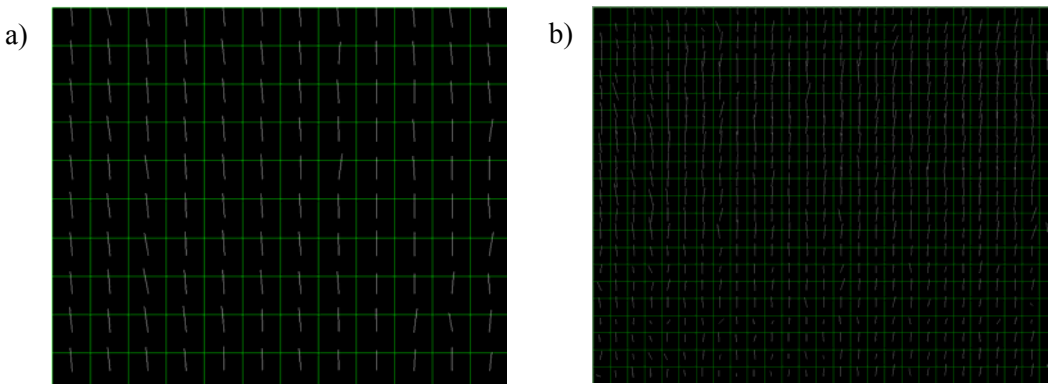

Figure 9. Distances between reference spots and displaced spots for: a) self-image. b) Triple spots frequency.

It is easily noticeable that for the same wavefront aberration, spot displacements are much larger in the self-image than in the other case due to the fact that we are taking the self-image further away from the LCoS display than in the triple frequency. This means that the focal length is larger and so, the setup is more sensitive to small aberrations of the initial wavefront.

Working with the self-image presents, in addition, other advantages. It is not well-known the way in which spots are formed in the double frequency or in the triple frequency. Intermediate spots may appear because of main spot interferences and so, the displacement of these recently generated spots could not provide real information about the wavefront aberration. Furthermore, working with bigger apertures greatly enhances the dynamic range.
The problem regarding lateral resolution and dynamic range of Shack-Hartmann sensors has been highly debated and it is an issue still not completely solved. Further studies will be oriented in this direction, trying to enhance the SH lateral resolution without implying dynamic range losses.
Finally, we show in Fig. 10. the spot displacements obtained when generating a Zernike polynomial.

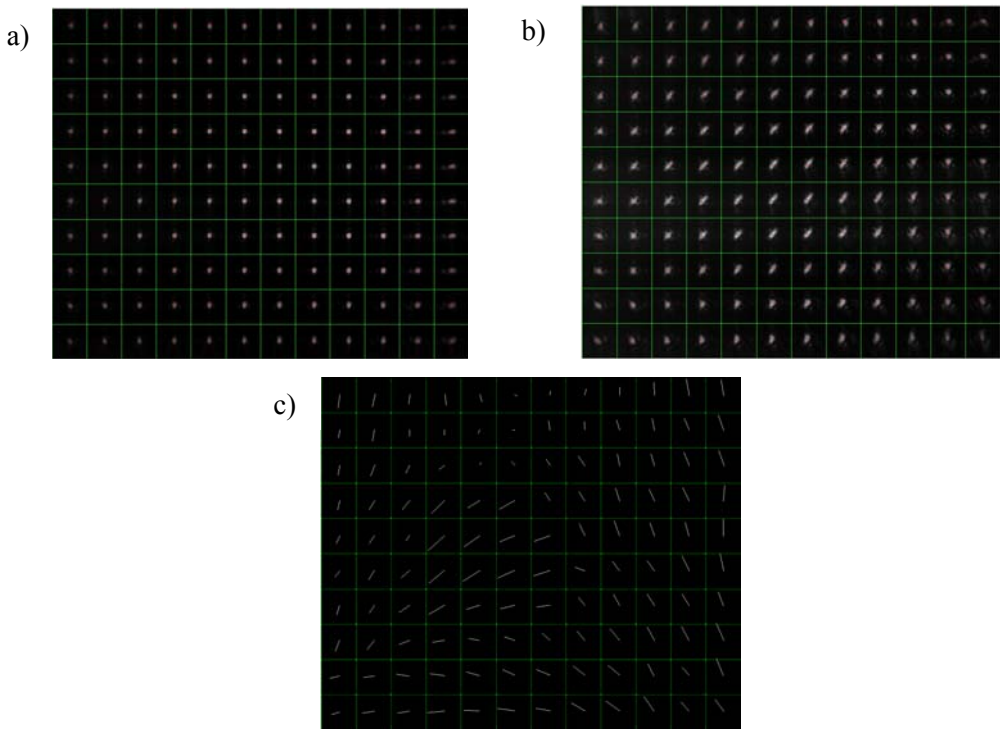

Figure 10. a) Reference spots with red crosses showing the centroid position. b) Displaced spots with red crosses showing the centroid estimation. The aberration corresponds to a third order Zernike polynomial with n=4 and l=2 in accordance with the ISO standard definition of Zernike polynomials. c) Distance between reference spots and displaced spots which provide information about the wavefront aberration.

The aberration of the wavefront experimentally measured in this example is a third order Zernike polynomial with n=4 and l=2 and a coefficient value of 50. Although the wavefront aberration is large and spots noticeable change their shape, it can be seen that the method applied to find the centroid location works properly and perfectly provides the final spot displacements shown in Fig. 10c). White segments in Fig. 10c) do not correspond to the real spots displacement since a magnifying factor of 5 has been added in order to be able to visualize the spots movement. The centroid estimation method here applied starts by finding the four central centroids, which are supposed to have the smallest aberrations, and from here, all the screen is swept by following a spiral. Zones with high intensity are allocated to a specific square and finally, the centre of mass of the determined square is found, resulting in the exact centroid position of the spot.

4. Conclusions

In this work we have conducted several studies. In the first one we conduct the optimization of a PA LCoS. In order to obtain good efficiencies when working in diffractive optics, the suitable electrical sequence must be addressed to the device. The chosen electrical pulse scheme must provide the largest possible global retardance as well as minimize time-fluctuations in phase.

Aberrations of the silicon substrate of the modulator must be as well taken into account and properly counteracted by addressing to the device the inverse phase function so that a perfectly flat wavefront can be generated when a flat wavefront comes into the LCoS display and is afterwards reflected. To determine the aberrations, we have made use of a Michelson interferometer and we have applied the phase-shifting interferometry because it provides highly accurate results.

Once the PA LCoS has been characterized and optimized, we have used it to generate the microlenses array of a Shack-Hartmann sensor. The entire sensor setup has been developed with the aim to determine wavefront aberrations, which in this case have been generated with a twisted nematic modulator. Experimental results show how important is the choice of a good collection of the parameters of the SH sensor which will definitely determine the dynamic range of the sensor, its sensibility to small aberrations and the lateral resolution of the device. Such parameters basically include the microlenses focal length, the aperture of these and the illumination wavelength. Furthermore, in order to obtain good results, a powerful method for the centroid estimation becomes essential too.

Our Shack-Hartmann sensor, built by means of a LCoS device, shows its validity to determine wavefront aberrations since the SH sensor parameters can be easily changed. Further studies will endeavour to increase the lateral resolution of these devices with a method non-implying dynamic range losses.

5. Acknowledgments

This research was funded by the Spanish Ministerio de Ciencia e Innovación through grant FIS209-13955-C02-01. I am indebted to my advisor, Prof. Juan Campos for his help and encouragement throughout the course of this work.

6. References

[1] S. T. Wu and D. K. Yang, [Reflective Liquid Crystal Displays], John Wiley & Sons Inc., Chichester, (2005).

[2] J. Turunen and F. Wyrowski Edts., [Diffractive Optics for Industrial and Commercial Applications], Akademie Verlag, Berlin, (1997).

[3] R. Dou and M. K. Giles, "Closed-loop adaptive optics system with a liquid crystal television as a phase retarder", Opt. Lett. 20, 1583-1585 (1995).

[4] W. Osten, C. Kohler and J. Liesener, "Evaluation and application of spatial light modulators for optical metrology", Opt. Pura Apl. 38, 71-81 (2005).

[5] A. De Martino, Y.K. Kim, E. Garcia-Caurel, B. Laude and B. Drévillon, "Optimized Mueller polarimeter with liquid crystal", Opt. Letters 28, 616-618 (2003).

[6] Anastasiadou, M., De Martino, A., Clement, D., Liège F., Laude-Boulesteix, B., Quang, N., Dreyfuss, J., Huynh, B., Nazac, A., Schwartz, L. and Cohen, H., A., S., "Polarimetric imaging for the diagnosis of cervical cancer", Phys. Stat. Sol. 5, 1423-1426 (2008).

[7] Jim Schiegerling and Edward DeHoog, "Problems testing diffractive intraocular lenses with Shack-Hartmann sensors", Appl. Opt. 49, D62-D68 (2010).

[8] Malacara D., [Optical shop testing], 3rd ed. New York. Chapter 10.

[9] J. R. Moore, N. Collings, W. A. Crossland, A. B. Davey, M. Evans, A. M. Jeziorska, M. Komarčević, R. J. Parker, T. D. Wilkinson and H. Xu, "The silicon backplane design for an LCOS polarization-insensitive phase hologram SLM", IEEE Photon. Techol. Lett. 20, 60-62 (2008).

[10] A. Lizana, I. Moreno, A. Márquez, C. Iemmi, E. Fernández, J. Campos and M. J. Yzuel, "Time fluctuations of the phase modulation in a liquid crystal on silicon display: characterization and effects in diffractive optics", Opt. Express 16, 16711-16722 (2008).

[11] I. Moreno, A. Lizana, J.Campos, A. Márquez, C. Iemmi and M.J. Yzuel, "Combined Mueller and Jones matrix method for the evaluation of the complex modulation in a liquid crystal on Silicon display", Opt. Letter 33, 627-629 (2008).

[12] Malacara D., [Optical shop testing]. 3rd ed. New York. Chapter 13.

[13] M. Rocktäschel and H.J. Tiziani, "Limitations of the Shack-Hartmann sensor for testing optical aspeherics", Optics & Laser Technology 34, 631-637 (2002).

[14] Yang Dai, Faquan Li, Xuewu Cheng, Zhiling Jiang and Shunsheng Gong, "Analysis on Shack-Hartmann wave-front sensor with Fourier optics", Optics & Laser Technology 39, 1374-1379 (2007).

[15] Ch. Siegel, F. Loewenthal and J.E. Balmer, "A wavefront sensor based on the fractional Talbot effect", Optics Communications 194, 265-275 (2001).